THE JOURNAL OF PHYSICAL CHEMISTRY C

Article

pubs.acs.org/JPCC

Electrical Resistance of Ag^{TS}–$S(CH_2)_{n-1}CH_3$//Ga_2O_3/EGaIn Tunneling Junctions

Ludovico Cademartiri,[†] Martin M. Thuo,[†] Christian A. Nijhuis,[†] William F. Reus,[†] Simon Tricard,[†] Jabulani R. Barber,[†] Rana N. S. Sodhi,*[,‡] Peter Brodersen,*[,‡] Choongik Kim,[†] Ryan C. Chiechi,[†] and George M. Whitesides*[,†]

[†]Department of Chemistry and Chemical Biology, Harvard University, 12 Oxford Street, Cambridge, Massachusetts 02138, United States, Wyss Institute for Biologically Inspired Engineering, Harvard University, 3 Blackfan Circle, Boston, Massachusetts 02115, United States, and Kavli Institute for Bionano Science & Technology, 29 Oxford Street, Cambridge Massachusetts 02138, United States

[‡]Surface Interface Ontario, Department of Chemical Engineering and Applied Chemistry, University of Toronto, 200 College Street, Toronto, ON, M5S 3E5, Canada

Supporting Information

ABSTRACT: Tunneling junctions having the structure Ag^{TS}–$S(CH_2)_{n-1}CH_3$//Ga_2O_3/EGaIn allow physical–organic studies of charge transport across self-assembled monolayers (SAMs). In ambient conditions, the surface of the liquid metal electrode (EGaIn, 75.5 wt % Ga, 24.5 wt % In, mp 15.7 °C) oxidizes and adsorbs——like other high-energy surfaces——adventitious contaminants. The interface between the EGaIn and the SAM thus includes a film of metal oxide, and probably also organic material adsorbed on this film; this interface will influence the properties and operation of the junctions. A combination of structural, chemical, and electrical characterizations leads to four conclusions about Ag^{TS}–$S(CH_2)_{n-1}CH_3$//Ga_2O_3/EGaIn junctions. (i) The oxide is ~0.7 nm thick on average, is composed mostly of Ga_2O_3, and appears to be self-limiting in its growth. (ii) The structure and composition (but not necessarily the contact area) of the junctions are conserved from junction to junction. (iii) The transport of charge through the junctions is dominated by the alkanethiolate SAM and not by the oxide or by the contaminants. (iv) The interface between the oxide and the eutectic alloy is rough at the micrometer scale.

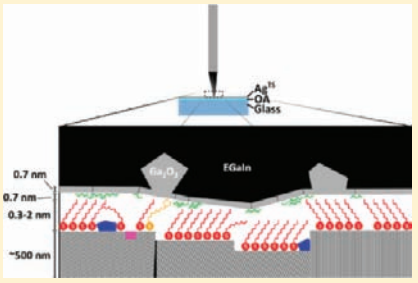

INTRODUCTION

We, and others, are developing procedures with which to study charge transport across self-assembled monolayers (SAMs).[1−32] We have explored two systems, both based on electrodes made of liquid metals (Hg, and a eutectic alloy of gallium and indium, which we abbreviate as EGaIn) and focused on the latter. The latter system has two major components: (i) a SAM supported by a template-stripped silver (Ag^{TS}) electrode and contacted by (ii) a "top" electrode of EGaIn (75.5 wt % Ga, 24.5 wt % In, mp 15.7 °C[33]) that is a liquid at room temperature and covered with a thin metal oxide film; we refer to these junctions by a nomenclature defined earlier[1] as Ag^{TS}–SR//Ga_2O_3/EGaIn, where R is an organic group (which may range in structure from simple *n*-alkyl groups to more complex functionalities, e.g., aromatics[28] or ferrocenes[13,34,35]).

These junctions are typically formed, characterized, and used in contact with ambient laboratory atmosphere. In these conditions, the surface of EGaIn oxidizes rapidly and spontaneously (for convenience we indicate the composite structure——oxide skin and metal electrode——as "Ga_2O_3/EGaIn") and it——as do all other surfaces——adsorbs adventitious contaminants (e.g., water, organic molecules, particles). The electrical resistance, thickness, and heterogeneity of the composite films of metal oxide and contaminants on the surface (and their variability from electrode to electrode, and from junction to junction) have not been characterized: the most serious ambiguity affecting the measurement of charge transport through Ag^{TS}–SR//Ga_2O_3/EGaIn junctions is currently the effect of the oxide skin and adventitious contaminants.[1,10,13,28,34,35]

Experimental efforts to understand charge transport across SAMs have been hampered by poor replicability caused, in part, by the difficulty of forming a reproducible electrical contact between a macroscopic electrode and a SAM. This poor reproducibility has both made it difficult to examine correlations between structure and conductance, and made it impractical to compare the results of measurements from techniques that operate under different conditions, and with different limitations (e.g., break junctions,[36] scanning probe microscopy,[37] Hg-drop junctions,[8,23,24,26,27,38] PEDOT:PSS junctions,[2,17] STM break junctions,[39−41] CP-AFM,[6,42] carbon electrode junctions,[43−46] or evaporated metal junctions[7,47]).

Received: December 27, 2011
Revised: February 25, 2012
Published: February 27, 2012

 © 2012 American Chemical Society

Table 1. Fundamental Characteristics of the Most Common Techniques for the Fabrication of Molecular Junctions[i]

Top contact	Junction	Yield of non-shorting junctions (%)	Toxic	Require clean room or major equipment	Performed in laboratory atmosphere[g]	Contact area	Ambiguities	β_N (C^{-1})[h]	Ref.
Hg drop	M-SAM//SAM-Hg	~50%[a]	Yes	No	Yes	250 μm^2	sel, env	0.51-1.04	8,12,22,24,25,27,55
	M-SAM//Hg	N/A						1.06	22,27
STM (tunneling)	M-CO_2H-C_n-CO_2H-M	N/A	No	Yes	Yes	SM	conf, geom, env	0.77-0.81	56
	M-S-C_n-S-M							0.5-1.04	56-58
	M-NH_2-C_n-NH_2-M							0.81-0.88	56
CP-AFM	M-SAM//M	N/A[b]	No	Yes	Yes	25 nm^2	int, num, for	0.88-1.17	4,6,18
	M-SC_nS-M						num, conf, geom, for	0.99	6,18
	M-SAM//NP-M						int, num, for	0.54-0.95	59,60
Evaporated metal	M-SAM//M	1.2 %	No	Yes[c]	Yes	7 μm^2	fab, int	0.8	14,48
Break junctions	M- SC_nS –M	N/A	No	Yes	Yes	SM	conf, env	1.0	40,49
Nanoparticle bridge	(NP-SC_n//)$_3$M	N/A	Yes[d]	Yes	No	N/A	num, sel, conf	0.79	5
Ga_2O_3/EGaIn	Ag^{TS}-SAM//Ga_2O_3/EGaIn	80-100%	No	No	Yes	N/A[e]	int, num	1.000 ± 0.015 (*even*) 1.033 ± 0.021 (*odd*)[f]	1,10,13,61
Carbon-based electrodes	PPF-$H_2NC_nNH_3$//M	90%	No	Yes	Yes	100 μm^2	int, conf, num, fab	1.1	19,44,45
Large-area junctions	M-SAM//PEDOT:PSS	~100%	No	Yes	Yes	100 μm^2	fab, int, env	0.66	2,15-17
NP arrays	M//(SC_nS-NP-M-SC_nS)$_n$//M	N/A	Yes	Yes	Yes	N/A	num, conf	N/A	62

[a]Within the first five traces. [b]In CP-AFM measurement the yield of the junction depends strongly on the pressure applied on the tip. [c]Evaporated electrodes require a clean room whenever high throughput (and, hence, patterning) is required. [d]Nanoparticles should be considered toxic especially when handled in their dry state. [e]While the area of contact of the EGaIn electrode on the SAM can be visually estimated (~100 μm^2), we do not have a direct measurement of the effective area of electrical contact, which is presumably smaller (25% of the visual estimate, according to a microscopy study[34]). [f]The two values of β were measured on alkanethiolate SAM containing, respectively, an even or odd number of carbons in the alkyl chain. [g]We define ambient conditions as either air or solution, on a laboratory workbench. [h]Usually β is not reported with error: when the error is reported, it is calculated differently by different laboratories. [i]NP = nanoparticle, C_n = alkyl chain, SAM = self-assembled monolayer, SM = single molecule. Positive traits of techniques are highlighted in green, and negative traits are highlighted in red.

The fact that few data have been analyzed for statistical significance, and that most sets of data are sparse,[10,13,34,48,49] due often (but not exclusively) to technical limitations, makes it difficult to evaluate and compare sets of data.[50,51]

In Table 1 we list and divide into eight categories the main kinds of ambiguities affecting the most common methods of measuring tunneling currents through molecules.

(i) *num*: The number of molecules that contribute to the total tunneling current cannot be determined experimentally.

(ii) *int*: The influence of the interface between the electrode/buffer layer and the molecules is uncertain. This uncertainty can arise from the type of contact between the molecules and the electrode/buffer layer, the exact composition of the electrode/buffer layer, or the electrical properties of the electrode/buffer layer.

(iii) *fab*: The influence of the fabrication process (e.g., photolithographic steps that are performed after the molecules are incorporated into the junction) on the structure of the SAM and/or on the conformation/structure of the molecules is not known.

(iv) *conf*: The conformation of the molecules in the junction is uncertain. This uncertainty includes the effect of mechanical stresses——due, for example, to electrostriction——that can be applied to the molecules inside the junction.

(v) *geom*: The geometry of the molecule−electrode complex is uncertain. For example, when thiols adsorb on the tips of metal probes (especially in AFM- and break-junction-based systems), it is not clear how/where they bind.

(vi) *for*. The effects that forces applied to the molecules in the junction (e.g., when a probe is brought into contact with a SAM using a piezoelectric drive in a feedback loop) have on the structure of the junction cannot be determined experimentally.

(vii) *env*: The effects of the local environment (e.g., the solvent bath in Hg drop junctions, or contaminants from the fabrication process) on the molecules in a junction are unclear.[52]

(viii) *sel*: The self-selection of data is inherent to the technique. For example, certain types of defects in a SAM cause the catastrophic failure of the junction and mask the influence of these defects on the data.

Figure 1 outlines the formation of Ag^{TS}−SR//Ga_2O_3/EGaIn junctions. We form the electrodes by stretching a droplet of Ga_2O_3/EGaIn between a syringe——which functions as a reservoir of fresh EGaIn——and a substrate to which the droplet adheres (Figure 1a,b). As we move the substrate away from the syringe with the help of a micromanipulator, the droplet elongates into an hourglass shape (Figure 1c), which eventually snaps at its thinnest point. This break generates two opposing tips: one hanging from the syringe and the other protruding from the substrate (Figure 1d). These tips do not spontaneously revert to a nearly spherical shape as expected for a liquid with high excess interfacial free energy (e.g., Hg). Instead they retain their conical profiles, apparently due to the

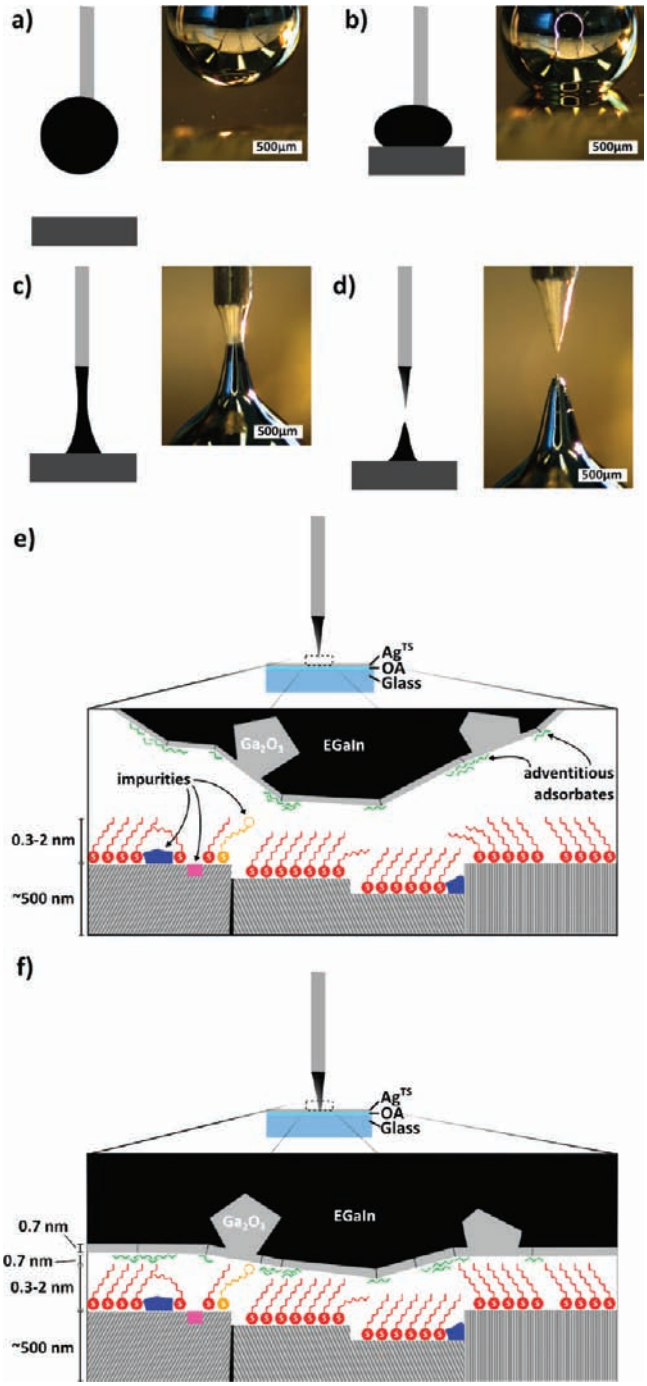

Figure 1. Formation of Ag^{TS}–SR//Ga_2O_3/EGaIn junctions. (a) A droplet is formed at the tip of a syringe filled with EGaIn. (b) Pushing the substrate against the droplet causes it to adhere. (c) Careful withdrawal of the substrate deforms first the droplet into an hourglass shape (the different colors in the two halves of the hourglass shape are due to the reflection of the gold substrate and dark ceiling——in these pictures we use this difference in color to improve the clarity of the image). (d) The hourglass-shaped droplet snaps eventually at its thinnest point, and forms two opposing tips. (e) The sacrificial substrate is removed and the SAM-covered Ag^{TS} substrate (supported on borosilicate glass by optical adhesive, OA) is placed under the new tip (in the inset, a diagram of the substrate before contact with the SAM shows the heterogeneities and defects that are present in the substrate, in the SAM, and in the tip; airborne contaminants and water molecules adsorbed on the oxide surface have been omitted for clarity). (f) The substrate is pushed in contact with the electrode (in the inset, a diagram of the junction shows the partially conformal deformation of the electrode).

noncompressible Ga_2O_3 skin.[53,54] With the help of a micromanipulator and a microscope (or a camera) connected to a monitor, we form the molecular junction by bringing a new substrate——this one supporting the SAM——in contact with the apex of the tip attached to the syringe (Figure 1e,f).

We estimate the upper bound of the area, A, of the electrical contact from the diameter, d, of the contact region shown by the microscope, assuming (by using $A = \pi(d/2)^2$) that the contact is circular in shape. The contact of the electrode with the SAM can be imperfectly conformal due to macroscopic buckling of the Ga_2O_3 layer. A microscopy study suggests that the area that is effectively in electrical contact is ~25% of the upper bound A.[34]

The exposure of the apex of the electrode to the laboratory atmosphere is not rigidly defined in our experimental protocol, because it is impossible to assign a fixed time to what is, for now, a manual procedure such as the formation of the junction. Nonetheless, in typical practice, ~1 min of time separates the formation of the tip and the formation of the junction. This degree of exposure also occurs whenever a junction is disassembled by separating the Ga_2O_3/EGaIn tip from one region of the SAM, and another junction is formed with the same tip in a different region. One tip is used typically to form five (standard in our most recent protocols) to 12 (occasionally in our early reports) junctions.

Oxide Film on the Surface of Liquid Metals and Liquid Metal Alloys. The studies of oxidized surfaces of liquid metals that are most relevant to this work were conducted on Ga,[63] In,[64] and the alloys Ga–In–Sn[65] and EGaIn.[1,53,66]

Liquid Ga. Regan et al. found by low-angle X-ray scattering that the oxide formed on the surface of liquid gallium (after exposure to oxygen at dosages between 10^4 and 10^5 Torr·s, under vacuum conditions) was a 0.5-nm-thick and atomically smooth layer.[63] The thickness of the film did not change within the range of oxygen dosages and temperatures (between room temperature and 573 K) that were tested. The oxide skin was found to be partially passivating; increasing dosages of oxygen (between 10^4 and 10^5 Torr·s) in a vacuum did not increase the thickness of the layer, but exposure to air at atmospheric pressure formed a macroscopic and rough oxide layer (the authors did not pursue a detailed characterization of those samples).

Liquid In. Tostmann et al. showed, using low-angle X-ray scattering, that the oxidation of liquid indium (in the same range of temperatures, pressures, and exposures to O_2 explored by Regan et al. on Ga) formed macroscopic oxide clumps rather than the smooth film observed on liquid Ga.[64] The authors interpreted this difference as evidence that the oxide skin on In was not passivating, while the one on Ga was.

Liquid Ga–In–Sn Alloy. Using X-ray photoelectron spectroscopy (XPS), Scharmann et al. found that the oxidation (by exposure to air for unspecified times at 303 ± 1 K, 1 atm, and between 9 and 95% relative humidity (RH)) of a Ga–In–Sn alloy[65] formed an oxide skin (a mixture of Ga_2O_3 and Ga_2O) whose thickness ranged between 1.9 and 2.5 nm, depending on the relative humidity.

Liquid EGaIn. Dumke et al. analyzed the surface of Ga_2O_3/EGaIn by ion sputtering and scanning Auger spectroscopy.[66]

dx.doi.org/10.1021/jp212501s | J. Phys. Chem. C 2012, 116, 10848–10860

They concluded that the oxide layer (formed in the ambient laboratory atmosphere after a few minutes of exposure) was mostly Ga_2O_3 and that, since the metal was visible by eye underneath, it was thinner than 10 monolayers; for the sake of expressing this estimation in SI units (~2 nm), we interpret here these "monolayers" to be the Ga−O bilayers in the Ga_2O_3 structure proposed by Regan at al. for the oxide skin on liquid Ga.[63] Our group has previously characterized the structure and composition of the surface of Ga_2O_3/EGaIn by Auger spectroscopy and by parallel-plate rheometry.[1,53] Our Auger spectra showed that the surface of Ga_2O_3/EGaIn was enriched in Ga, compared to the bulk alloy. After sputtering to remove the oxide, the surface was instead enriched in In. Exposure to ambient air caused the surface to revert to the original Ga-enriched state. Our rheometry data showed that the yield stress of Ga_2O_3/EGaIn did not change over time.[53,54] In our interpretation, these results suggested that the oxide on EGaIn was mostly composed of gallium oxides (hence the Ga_2O_3/EGaIn nomenclature), that In segregates to the interface between the liquid alloy and the oxide,[67] and that the oxide is passivating.

Electrical Characteristics of the Surface Layer Formed on EGaIn in Air. The electrical properties of Ga_2O_3 have been extensively studied in the past.[68−70] Resistivity of pure crystals of β-Ga_2O_3 have been reported between 1 Ω·cm (when they are grown from Ga_2O_3 dissolved in pure Ga)[68] and ~10^{10} Ω·cm (when grown as epitaxial thin films on GaAs).[70] The resistivity of thin (4−400 nm) films of Ga_2O_3 deposited by electron-beam evaporation was reported to be 10^{12}−10^{13} Ω·cm.[69] The extraordinarily large range of resistivities displayed by Ga_2O_3 makes it difficult to compare the resistivities or resistances of the oxide formed on EGaIn and of Ga_2O_3 crystals.

Comparably accurate studies on the electrical characteristics of the surface layer (i.e., oxide + adventitious contaminants) formed on EGaIn in air are missing due to the difficulty of establishing a well-defined and reliable contact with a thin oxide skin on a liquid surface. Our group has reported estimations in previous papers.[13,34] Nijhuis et al. estimated the resistance of the surface layer on an EGaIn drop by comparing the transport of charge between two copper wire electrodes in three different configurations.[13] (i) In the first configuration (open circuit), both copper wires penetrated the oxide skin of the same droplet of EGaIn; a bias applied to the copper wires showed metallic conduction through the eutectic alloy. (ii) In the second configuration, one wire penetrated the oxide skin of a droplet of EGaIn, while the other touched its surface; transport of charge between the two wires occurred through one surface layer. (iii) In the third configuration, both wires contacted the surface of the same droplet of EGaIn; charge transport occurred through two surface layers. Those experiments showed that the surface layer on a Ga_2O_3/EGaIn drop was ~2 orders of magnitude more resistive than the rest of the circuit, including the bulk EGaIn. In a later paper, Nijhuis et al. also measured the temperature dependence (between 260 and 295 K) of the resistance of the surface layer on a Ga_2O_3/EGaIn drop again by the copper wire scheme;[34] the transport of charge was thermally activated within the range of temperatures explored. In a dielectric, a dependence of charge transport on temperature suggests that tunneling is not the dominant mechanism of charge transport. (Nonetheless, one has to be careful about the contribution of interfaces and adventitious contaminants on the temperature dependence of $J(V)$.)

Motivation for this Study. The two most serious ambiguities of Ag^{TS}−SR//Ga_2O_3/EGaIn junctions lie with the surface of the top electrode: specifically, (i) the absolute contribution of the oxide and of the adventitious contaminants to the resistance of the junction is unclear (we have typically focused on studies that compare paired measurements on the same junctions——e.g., rectification——in order to alleviate this problem[10,13]), and (ii) the effect of environmental or procedural variables (e.g., manipulation, length of exposure to air, sharpness of the tip) on the resistance of the surface of the electrode is complicated and still undefined. These electrical unknowns (e.g., resistance of oxide, adventitious contaminants, and interfaces) derive in part from structural and chemical unknowns (e.g., the thickness and composition of the oxide and their uniformity and reproducibility, the nature of the interface between the oxide and the SAM, the distribution, composition, and typical thickness of adventitious contaminants on the tip), and result in ambiguities in the measurement of the $J(V)$ characteristics of SAMs with Ga_2O_3/EGaIn top electrodes. Understanding the structure and composition (and, therefore, the resistance) of the surface of Ga_2O_3/EGaIn in ambient atmosphere is an important and necessary step in developing the Ga_2O_3/EGaIn electrode as a tool for characterizing the tunneling properties of SAMs.[1,10,13,28,34]

This paper elucidates the composition and structure of the surface of Ga_2O_3/EGaIn electrodes and, by extension, clarifies the composition and structure of Ag^{TS}−SR//Ga_2O_3/EGaIn tunneling junctions. The oxide skin is apparently passivating, ~0.7 nm thick (on average), predominantly composed of Ga_2O_3, and, importantly, unaffected by its curvature (between radii of curvature of ~50 μm and ~1 cm) and its history of exposure to repeated deformations (between 0 and 25 deformations). The adventitious contaminants consist largely of partially oxidized aliphatic chains (0.7 nm thick, on average, after ~1 h in laboratory air) and water (likely two to four layers of molecular water at typical laboratory relative humidities, i.e., 20−60%).

These results allow us to estimate the upper bound of the resistance (~10^3 Ω) of the surface layer (i.e., metal oxide + adventitious contaminants) on the contacting surface of the "Ga_2O_3/EGaIn" electrode. This maximum resistance is ~4 orders of magnitude smaller (at 0.5 V bias) than that of the least resistive alkanethiolate SAM-based junction we have measured so far (Ag^{TS}−$S(CH_2)_9CH_3$//Ga_2O_3/EGaIn). These results help define the range of applicability of these junctions for physical−organic studies of charge transport through organic molecules.

EXPERIMENTAL DESIGN

Samples. We were interested in assessing the influence of the curvature and of the history of deformations on the composition and structure of the surface of Ga_2O_3/EGaIn. To this end, we characterized three kinds of samples.

"Fresh" Tips. We fabricated (in laboratory atmosphere, and at room temperature) electrodes in the form of tips (seven replicates), by the four-step procedure introduced earlier[1] and detailed in the Methods section in the Supporting Information. These tips differed from those used as top electrodes in molecular junctions in that they were pointing upward instead of downward (which affects the roughness of the surface), were exposed to laboratory atmosphere for a longer time (~1 h, they were probably more contaminated than the electrodes used in molecular junctions), and were exposed to the XPS sample

dx.doi.org/10.1021/jp212501s | J. Phys. Chem. C 2012, 116, 10848−10860

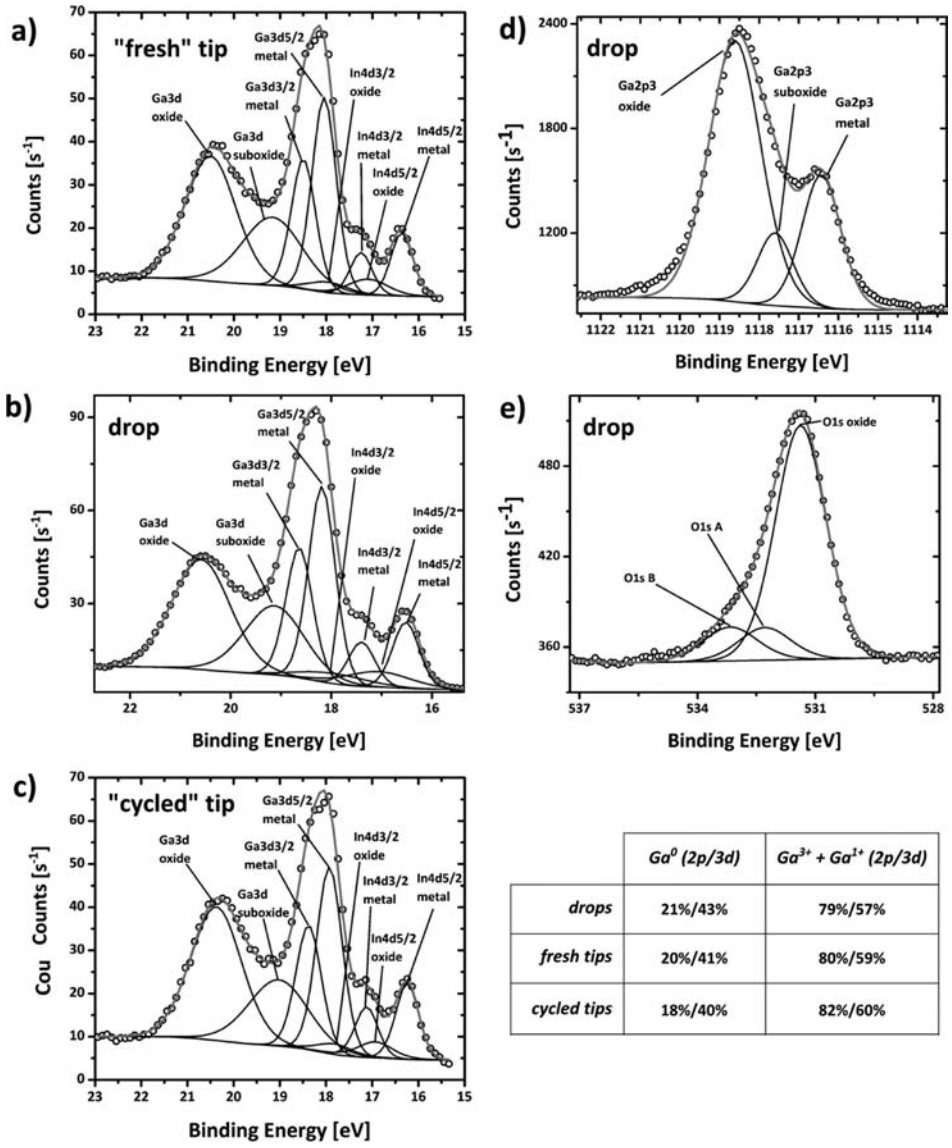

	Ga^0 (2p/3d)	$Ga^{3+} + Ga^{1+}$ (2p/3d)
drops	21%/43%	79%/57%
fresh tips	20%/41%	80%/59%
cycled tips	18%/40%	82%/60%

Figure 2. Composition of the oxide layer. (a–c) High-resolution XPS spectra of the Ga 3d/In 4d region collected from the apex of samples of Ga_2O_3/EGaIn: a "fresh" tip ($r \sim 10^2$ μm), a drop ($r \sim 1$ cm), and a tip that has undergone 25 cycles of reversible deformations. (d) High-resolution XPS spectrum of the Ga 2p region collected from the apex of a drop of Ga_2O_3/EGaIn indicated the presence of three species of gallium (Ga_2O_3 species, Ga_2O species, and metallic gallium). (e) High-resolution XPS spectrum of the O 1s region collected from the apex of a drop of Ga_2O_3/EGaIn and indicating the presence of three species of oxygen (attributed to oxides, hydroxyls, and oxidized carbon). The table compares the atomic percentages of Ga metal (Ga^0) and Ga oxide/suboxide (Ga^{3+} + Ga^+) obtained from the fitting of XPS Ga 2p and Ga 3d signals from drop samples, fresh tips, and cycled tips.

exchange chamber (which can be a source of adventitious contamination[71,72]).

"Cycled" Tips. We assessed the influence of the history of deformations on the surface of Ga_2O_3/EGaIn by deforming repeatedly (25 times) a number of tips (seven replicates). The deformations were achieved by bringing the two opposing tips that formed after the fracture of the hourglass shape against each other. Visible deformations that occurred at the edges of the contact indicated mechanical contact between the tips. Sufficiently small deformations did not weld together the two tips. Upon separation, the opposing tips appeared to revert to the original shape.

Drops. Ga_2O_3/EGaIn, spread on a flat glass substrate with a syringe, formed drops with a diameter of ~1 cm and a radius of curvature of ~1 cm. The radius of curvature of these samples (~1 cm) is approximately 2 orders of magnitude larger than that of the tips used in junctions. We used this difference to infer the influence of curvature on the composition and structure of the Ga_2O_3/EGaIn surface by comparing the XPS data collected from the apex of the curved surface of the drops and the tips.

Techniques. We characterized the apex of these samples using XPS and time-of-flight secondary ion mass spectrometry (ToF-SIMS). The choice of these experimental techniques was based on their ability to characterize the average chemical composition of the surface of a solid oxide film supported on a nonvolatile liquid material as a function of depth. The Supporting Information describes the details.

RESULTS AND DISCUSSION

Composition of the Surface Oxide. In all samples, the survey XPS analysis showed only signals from C, O, Ga, and In

dx.doi.org/10.1021/jp212501s | J. Phys. Chem. C 2012, 116, 10848–10860

atoms. Figure 2a−c shows the high-resolution XPS spectra of the Ga 3d and In 4d peaks collected from the "fresh" tips, the "drops", and the "cycled" tips. Our assignments of the peaks are consistent among all samples, and with literature values.[73] For Ga, we observed Ga^0 (doublet centered at ~18.2 eV), which we associate with the EGaIn alloy, Ga^+ (~19 eV), which we associate with Ga_2O, and Ga^{3+} (~20.5 eV), which we associate with Ga_2O_3. (The assignments of the Ga signals were confirmed by the high-resolution XPS spectrum of the Ga 2p peaks shown in Figure 2d.[74]) For In, we observed In^0 (doublet at ~16.3 and ~17.3 eV), which we associate with the EGaIn alloy, and In^{3+} (doublet at ~17.1 and ~18 eV), which we associated with In_2O_3, after comparison to a In_2O_3 standard. The composition profile of the three types of samples——"drop", "fresh tip", and "cycled tip" (table in Figure 2)——is within the error expected from XPS. (The ratio of oxide to metal is different when considering the Ga 2p or the Ga 3d levels due to the relative escape depths of these two types of photoelectrons; this difference is reflected in different sampling depths.) The similarity of these compositional profiles indicates that neither reversible deformations nor the curvature of the electrode affects the composition or the average thickness of the oxide layer; angstrom-scale differences in the average thickness of the oxide layer would result in observable differences in the ratios between the intensities of the Ga^{3+} and Ga^0 XPS signals.[75,76] While deformations have an effect on the mechanical properties of the surface,[54] and might plausibly have a macroscopic effect on its roughness (and thus on the effective contact area of the junctions), the nanoscopic characteristics (i.e., composition and thickness of the layer of oxides and contaminants) of the surface, and thus of the junctions, are——according to these XPS results——unaffected by the history of handling and by the shape of the electrode.

The O 1s region of the spectrum showed a minimum of three species of oxygen (Figure 2e); while the shape of the peak could be deconvoluted well with a minimum of three peaks, it is likely that the samples contain more than three species of oxygen. We attributed the first peak (530.8 eV, O 1s) to the inorganic oxides of gallium and indium. The remaining two peaks at higher binding energies (531.5 eV, O 1s A, and 532.8 eV, O 1s B) are likely produced by hydroxyl groups and organic oxygens, but cannot be attributed unambiguously.

Thickness of the Oxide Skin. The compositional profile of the oxide skin was determined by angle-resolved XPS (ARXPS) and ToF-SIMS. Both analyses could only be performed on drops of Ga_2O_3/EGaIn. In the case of XPS, the apex of the tips had a curvature comparable to the spot size of these techniques. In the case of ToF-SIMS, the tips collapsed under sputtering, upon removal of the oxide layer; cooling the tips below the melting point of the alloy also caused the tips to collapse. The data shown in Figure 2, however, demonstrate that the average thicknesses of the oxide layer (and thus its structure) in the drop and tip samples are indistinguishable by XPS.

ARXPS characterizes the variation of the intensity of an XPS signal with the angle of detection (defined here as the angle between the direction of detection and the normal to the surface). Electrons detected perpendicularly to the surface (i.e., at 0°) originate from a volume of material which is proximal to the surface and whose thickness is approximately equal to the escape depth of electrons. Electrons detected at angles other than the normal to the surface will have, on average, escaped from a volume of material closer to the surface, and will therefore be more representative of the composition at the surface. A dependence of the intensity (usually plotted in units of atomic fraction) of an XPS signal on the angle of collection indicates that the species responsible for that signal are not homogeneously distributed in the volume being probed, but are instead heterogeneous with depth. ARXPS cannot give comparably accurate information describing the lateral distribution of the species: most models used to simulate ARXPS data assume that the surface is adequately approximated as a stack of layers of different thicknesses and compositions.

The derivative of the dependence of the atom fraction on the collection angle indicates if a species is localized at the surface (positive slope) or deeper in the material (negative slope); normalized data from multiple signals are often plotted in the same graph to compare the relative vertical distribution of the species assigned to those signals. Figure 3a shows the ARXPS data from the C and O species. The signal from C decreases with decreasing angle, while the signal from the inorganic oxides increases with decreasing angle. These opposite trends indicate that the adsorbed organic contaminants are localized above the oxide (O 1s signal), as expected. The other oxygen signals (O 1s A and O 1s B) had a much smaller dependence on the angle of collection. The signals associated with the C 1s orbital showed indistinguishable dependencies on the angle of detection (data not shown). Figure 3b shows the ARXPS data that compare Ga and In species. The signals from Ga^{3+} and Ga^0 have opposite slope; Ga_2O_3 is located, on average, above the alloy. The signals from In^{3+} and In^0 have similar dependencies on the angle of detection; In_2O_3 and In are both localized below Ga_2O_3.

Relative depth profiles (RDPs) provide a semiquantitative way of summarizing ARXPS data.[77] The relative depth (RD_i) of a chemical species i is calculated as $RD_i = \log(I^i_{\theta 1}/I^i_{\theta 2})$, where $I^i_{\theta 1}$ and $I^i_{\theta 2}$ are the intensities of the XPS signals from the species i collected at angles $\theta 1$ and $\theta 2$ from the normal to the surface, and $\theta 1 > \theta 2$ (i.e., $\theta 1$ is more surface sensitive than $\theta 2$). (Compared to other approaches, RDPs avoid making assumptions about the structure of the surface, or about the lateral distribution of the species.) The result of this analysis is a plot of the relative depth, RD, for all the species we detected (Figure 3c), sorted on the abscissa in order of increasing relative depth. The organic contaminants associated with C 1s were the outermost species, followed by the oxygens associated with the O 1s A and O 1s B signals (tentatively attributed to organic oxygens and hydroxyls). Beneath these species, in order of increasing depth, we found Ga_2O_3 (i.e., signals from Ga^{3+} and O 1s), Ga_2O (i.e., signal from Ga^+), In_2O_3 (i.e., signal from In^{3+}), and the eutectic alloy (i.e., signals from both In^0 and Ga^0).

A calculation of the thickness of the oxide, which for the purposes of this calculation was not including In_2O_3, indicated that the average thickness was on the order of 0.7 nm. More specifically, since the ratio of O to Ga^{3+} + Ga^+ remained fairly constant with the angle, the fraction of Ga associated with this "pure" layer can be equated to I^0_{Ox} (43%). Further, taking the value of Ga from the eutectic composition (I^0_{Met} = 84%), a single-overlayer model could be applied in the same manner as described by Jedral et al.[78] resulting in this estimate. While this value is consistent with the one (0.5 nm) obtained by X-ray scattering from the Ga_2O_3 layer formed on oxidized liquid gallium,[55] those experiments were performed in high-vacuum conditions. The same authors reported that Ga develops an

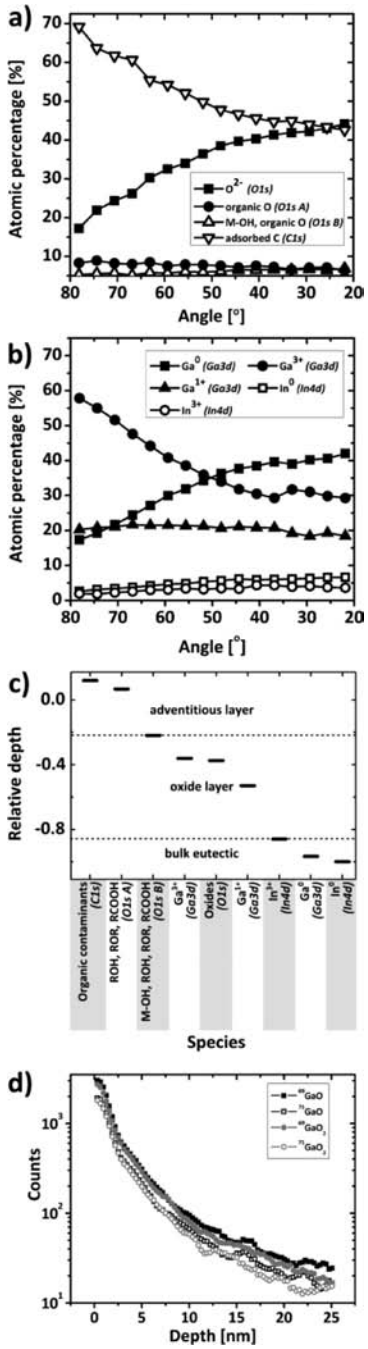

Figure 3. Structure of the surface of Ga_2O_3/EGaIn in ambient conditions. (a) ARXPS profile of the C and O species collected from a drop of Ga_2O_3/EGaIn (signals at higher angles on the abscissa are more sensitive to the surface); (b) ARXPS profile of the Ga and In species collected from a drop of Ga_2O_3/EGaIn (signals at higher angles on the abscissa are more sensitive to the surface); (c) relative depths of the main species identified by XPS. The relative depth is a dimensionless number ($RD_i = \log(I^i_{\theta 1}/I^i_{\theta 2})$, where $I^i_{\theta 1}$ and $I^i_{\theta 2}$ are the intensities of the XPS signals from the species i collected at angles $\theta 1$ and $\theta 2$, and $\theta 1 > \theta 2$) that is related to the average depth of origin of the signal from a species. This calculation does not make assumptions about the structure of the surface; here, we assume that the surface is, in a first approximation, a stack of layers with homogeneous composition. The compositions shown were calculated from the ARXPS data collected from the drop of Ga_2O_3/EGaIn. (d) ToF-SIMS depth profile of the drop of Ga_2O_3/EGaIn, for four fragments associated with Ga_2O_3.

oxide layer of macroscopic thickness when exposed to ambient atmosphere. Therefore, the apparently passivating character and the remarkable thinness of the oxide skin formed on EGaIn in air are, to a certain degree, surprising. The average thickness of the oxide obtained by ARXPS was validated by ToF-SIMS. Figure 3d shows the abundance of the four most abundant oxide fragments as a function of depth (in nanometers) for the drop sample; we conclude from the profile that the thickness of the oxide is no more than 2−3 nm, consistent with the estimation from ARXPS.

Topography of the Ga_2O_3/EGaIn Interface. The analysis of the ARXPS data yielded a value of thickness for the oxide layer which is averaged over the spot size from which electrons are collected (100 μm). We were interested in characterizing the heterogeneities in the thickness of the oxide layer over dimensions relevant to the scale of the molecular junctions (~100 μm in radius). To this end, we measured the two-dimensional map of the intensity of $^{71}GaO_2^-$ fragments ejected from the surface of a frozen drop of Ga_2O_3/EGaIn, as the sputtering progressed. (The drop had to be frozen to −25 °C; upon sputtering of the oxide layer, the liquid drop of EGaIn reverted to the shape with minimal surface energy expected from high surface energy liquids.) The thinnest regions (thickness of 0.7 nm) of the oxide film were removed first, thus exposing the bulk eutectic, decorated by threadlike islands of thicker oxide. The resulting map is shown in Figure 4 (the lighter the tone, the higher the count rate of $^{71}GaO_2^-$ fragments).

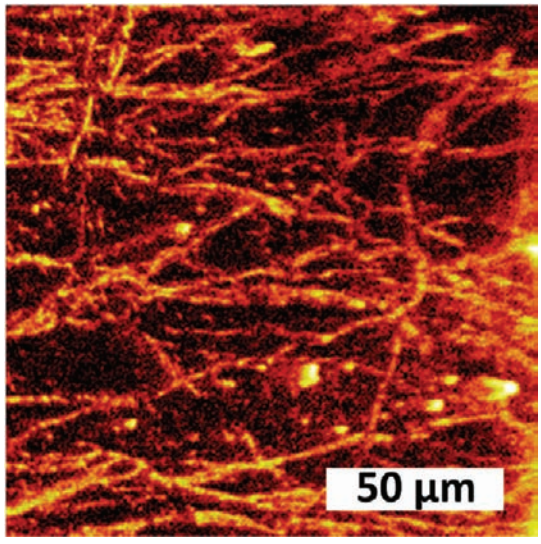

Figure 4. ToF-SIMS analysis of inhomogeneity in the thickness of the oxide layer. $^{71}GaO_2^-$ signal from the bottom of the sputter crater produced on a Ga_2O_3/EGaIn drop sample (the dimensions of the imaged area are 151 μm × 151 μm) after the thin fraction of the oxide skin has been sputtered away; the lines indicate regions of thicker oxide. The lines are ~3−4 μm in width.

While the majority of the surface of the bulk eutectic is coated with a thin (~0.7 nm) layer of oxide, Figure 4 shows that the oxide skin is heterogeneous. These heterogeneities, which appear in the form of threads ~3−4 μm wide, could be due, in part, to the freezing of the droplet or handling. We were able to observe the surface of the drop during its solidification and the formation of corrugations on the surface as the temperature was lowered.[79]

dx.doi.org/10.1021/jp212501s | J. Phys. Chem. C 2012, 116, 10848−10860

Thickness, Nature, and Characteristics of the Adventitious Layer. Figure 5a shows the HRXPS spectrum of the C 1s region obtained from the "drop" sample. We deconvoluted the signal into four peaks at 284.70 eV (set as the binding energy reference and attributed to methylene carbons), 286.34 eV (compatible with ethers), 287.91 eV (compatible with alcohols), and 289.03 eV (compatible with C═O groups). The table in Figure 5 shows the atomic fractions of the species. The fraction of carbon atoms that was bound to at least one oxygen was approximately 17%, consistent with the observations of Barr and Seal (10−30%[80]).

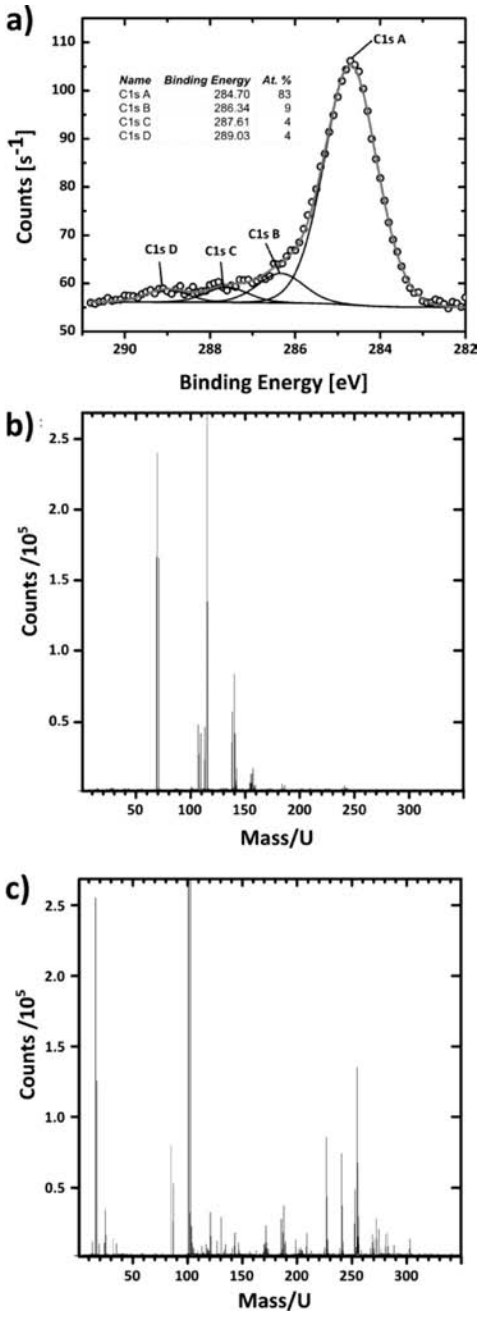

Figure 5. Chemical analysis of the adventitious carbon. (a) High-resolution XPS spectrum of the C 1s peak collected from a drop of Ga_2O_3/EGaIn. The table on the left shows the atomic percentages of the four species of carbon identified in the deconvolution. (b) ToF-SIMS survey spectrum obtained from a drop of Ga_2O_3/EGaIn characterized in April 2010. (c) ToF-SIMS survey spectrum obtained from a drop of Ga_2O_3/EGaIn characterized in November 2009.

The amount and nature of the contaminants strongly depended on the environmental conditions. Parts b and c, respectively, of Figure 5 show the ToF-SIMS total ion current survey spectrum from the drop samples during analyses conducted in April 2010 and November 2009 on the same instrument. In the November experiments, we detected a series of fatty acids (C_9−C_{22}). In April, however, the mass spectra were cleaner and dominated by the inorganic fragments, while no particular organic functional group (e.g., carboxylic acids, nitriles, amines, thiols, phenyls) seemed to dominate the organic fragments.

On average, the typically expected adventitious C layer was estimated to be ∼0.7 nm by using a single-overlayer model[78] with I^0_{Ox} (43%) for Ga. This value of thickness is consistent with the one (0.3−0.9 nm) measured on Al_2O_3/Al by Piao and McIntyre.[81] The duration of the exposure to ambient laboratory atmosphere (∼1 h) was dictated by the experimental (e.g., fabrication of multiple tips on a single substrate as replicates) and instrumental (e.g., mounting the sample on the sample holder of the XPS, inserting the sample, degassing) protocols. When Ga_2O_3/EGaIn is used as a conical tip electrode in molecular junctions, its exposure to ambient conditions is typically much shorter than 1 h (∼5 min: each tip is used to make ∼5 junctions and each junction takes ∼1 min to make).[13] We can, therefore, expect that this amount of contamination is larger than or equal to that found in the junctions.

Influence of the Oxide on the Transport of Charge through the Junctions. Regardless of the mechanistic details of charge transport, all elements in a SAM-based molecular junction (in the case of Ag^{TS}−SR//Ga_2O_3/EGaIn junctions, the oxide layer, the adventitious contaminants, the SAM, and the interfaces) can be thought of as a combination of resistors in series and in parallel. If we assume the junction to be parallel to the *xy* plane of a Cartesian coordinate system and that charge transport occurs only in a direction perpendicular to this *xy* plane, each infinitesimal element of the junction $t{\cdot}dx{\cdot}dy$ (where *t* is the thickness of the junction) can be considered as a series of resistors (in the case of Ag^{TS}−SR//Ga_2O_3/EGaIn junctions, the bottom electrode, the SAM, the van der Waals contact, the organic contaminant, the oxides, and the bulk metal) with different resistances (due to their different thicknesses, compositions, and structures); if the resistances of these resistors are sufficiently different at a particular bias, the resistance of the $t{\cdot}dx{\cdot}dy$ element perpendicular to the *xy* plane is dominated by the most resistive layer within it (because the total resistance of $t{\cdot}dx{\cdot}dy$ is $r_{tot} = r_1 + r_2 + r_3 + ... + r_i$, where *i* is here the number of layers and the *r* are the resistances of each layer). In the junction, all these infinitesimal $t{\cdot}dx{\cdot}dy$ elements are parallel to each other. The resistance of the junction will, therefore, be determined by the least resistive areas ("thin areas"[12]), because $1/R_{tot} = 1/R_1 + 1/R_2 + 1/R_3 + ... + 1/R$, where the *R* are the resistances of each $t{\cdot}dx{\cdot}dy$ element comprising the junction. This feature is common to SAM-based molecular junctions, where thin-area and thick-area defects are always present and parallel to each other.[12]

Since the thinnest areas dominate the charge transport through the junction,[12] but the resistance of each area is dominated by its the most resistive element, we only consider in the following discussion the areas of the junction where the surface layer is thinnest and yet displays all the elements that

dx.doi.org/10.1021/jp212501s | J. Phys. Chem. C 2012, 116, 10848−10860

could be contributing to charge transport (i.e., 0.7-nm-thick oxide layer, 0.7-nm-thick adventitious layer).

Estimating the resistances of the individual elements is difficult, in part because it is currently experimentally impossible to measure the contribution of the electrical contacts. The resistance of the metal oxide on EGaIn could not be extracted from our measurements of its electrical characteristics, because adventitious contamination and contact resistances were present in all of the measurements.[13,34] Nonetheless it is possible to estimate the resistance of the surface layer (i.e., oxide, adventitious contaminants, and interfaces) from an analysis of the J obtained at a chosen bias from $Ag^{TS}-S(CH_2)_{n-1}CH_3//Ga_2O_3/EGaIn$ junctions of different thicknesses (e.g., different values of n). The conduction of charge through SAMs in $Ag^{TS}-S(CH_2)_{n-1}CH_3//Ga_2O_3/EGaIn$ junctions is dominated by tunneling.[1,10] The rate of tunneling is described, to a first approximation, by a simplification of the Simmons equation[82] in the form $J(V,d) = J_0(V) \exp[-\beta(V)d(V)]$, where V is the bias, d is the thickness of the tunneling barrier (which may be a function of V via electrostriction), and $J_0(V)$ is the hypothetical value of J at $d = 0$.[83] A comparison of $J(V)$ characteristics of $Ag^{TS}-S(CH_2)_{n-1}CH_3//Ga_2O_3/EGaIn$ junctions of different thicknesses (e.g., different values of n) can, therefore, (i) determine the characteristic "tunneling resistance" to tunneling (the decay constant β) of the SAM and (ii) collect in one parameter (J_0) the contribution of electrical contacts and other nuances of the junction (in the case of $Ag^{TS}-S(CH_2)_{n-1}CH_3//Ga_2O_3/EGaIn$ junctions, J_0 should be an estimate of the current density that would cross the junction in the absence of the SAM). Knowledge of the bias and of the contact area of the junction allows the determination, from J_0, of the resistance of the entire circuit surrounding the SAM. We know from previous experiments that, in the absence of the SAM, the surface layer on the electrode is the largest contributor to the resistance of the circuit.[34] Therefore, the resistance that we estimate from J_0 is a good estimate of the resistance of the surface layer on the electrode. This "surface" resistance can be then compared to that of the entire junction; this comparison allows us to infer the influence of the surface of the electrode on the charge transport in the junction, regardless of the mechanistic details of charge transport through the surface layer.

Due to the uncertainties (e.g., influence of interfaces and adventitious contaminants) associated with these resistances, we consider here the limiting case in which (i) the resistance of the surface layer is the largest that is still compatible with experimental results, and (ii) the resistance of the SAM is the smallest that is still compatible with experimental results. We calculate (using $R_{sl} = V_{sl}/(J_0A)$) the maximum resistance of the surface layer R_{sl} as $\sim 1 \times 10^3\ \Omega$, by using a conservative overestimation of the voltage drop across the surface layer (V_{sl} overestimated as 0.5 V; it is most likely orders of magnitude less than that) and a contact area A of 500 μm^2.

The shortest——and therefore least resistive——alkanethiolate that we have characterized with Ga_2O_3/EGaIn-based junctions is a SAM of $HS(CH_2)_9CH_3$, on a Ag substrate. The resistance of the $Ag^{TS}-S(CH_2)_9CH_3//Ga_2O_3/EGaIn$ junction at 0.5 V was $\sim 10^7\ \Omega$. Using a thickness of 1.1 nm for the SAM, and the maximum resistance ($\sim 10^{24}\ \Omega$) for the skin, we estimate the resistance of $S(CH_2)_9CH_3$ at 0.5 V to be $\sim 1 \times 10^7\ \Omega$.

In conclusion, the most resistive surface layer compatible with our experimental results is still approximately 4 orders of magnitude *less* resistive than the *least* resistive SAM we measured in $Ag^{TS}-S(CH_2)_{n-1}CH_3//Ga_2O_3/EGaIn$ junctions; *the values of J measured with $Ag^{TS}-S(CH_2)_{n-1}CH_3//Ga_2O_3/EGaIn$ junctions are not dominated by the surface of the $Ga_2O_3/EGaIn$ electrodes.*

In addition to estimating the relative contribution of the surface layer to the total resistance of EGaIn-based junctions, it is instructive to put these values in context by comparing them to those observed with other kinds of junctions. Of the many methods for constructing tunneling junctions, the two that are the most relevant to $Ag^{TS}-S(CH_2)_{n-1}CH_3//Ga_2O_3/EGaIn$ junctions are $Au-S(CH_2)_nSH//PEDOT:PSS$ junctions and Ag−SR//Hg junctions. These two kinds of junctions are similar to EGaIn-based junctions in that they (i) characterize SAMs formed on Au or Ag substrates, (ii) contain a van der Waals interface at one electrode, and (iii) form comparable areas of contact (the areas of the junctions are also measured directly, by microscopy). The magnitude of J for $Ag^{TS}-S(CH_2)_9CH_3//Ga_2O_3/EGaIn$ at 0.5 V bias is 10^{-2} A/cm^2.[10] The magnitude of J for the equivalent large-area junction, $Au-S(CH_2)_{10}SH//PEDOT:PSS$, is 10^1 A/cm^2.[2] Data for methyl-terminated SAMs are only available for $Au-S(CH_2)_{15}CH_3//PEDOT:PSS$, but showed abnormally high values of $J \sim 10^1$ A/cm^2 which were attributed to processing issues.[84] Wang et al. recently reported $J \sim 10^0$ and 10^{-1} A/cm^2 at 0.5 V for $Au-S(CH_2)_8SH//PEDOT:PSS$ and $Au-S(CH_2)_{12}SH//PEDOT:PSS$, respectively.[85] The magnitude of J for both $Hg-S(CH_2)_9CH_3//Hg$ and $Ag-S(CH_2)_9CH_3//Hg$ is 10^1 A/cm^2 at 0.4 and 0.2 V, respectively.[28,55] Thus, EGaIn-based junctions yield values of J that are consistently $\sim 10^3$ A/cm^3 lower than for comparable junctions, which is in excellent agreement with our estimations of the influence of the surface layer.

Influence of the Adventitious Contaminants on the Transport of Charge through the Junctions. Our data suggest that adventitious carbon consists mostly of aliphatic organic molecules that are partially oxidized (e.g., ROH or RCOOH, where R is an aliphatic group).[80] Most aliphatic molecules are electrically insulating in the bulk, but their contributions to the total resistance of tunneling junctions vary with their length and how they are oriented with respect to the electrodes.[86]

Although we cannot determine the structure of the adventitious adsorbates experimentally, we know the following experimental facts: (i) the apparent average thickness of these adsorbates (after 1 h of ambient exposure in a laboratory and loading into the XPS exchange chamber) is on the order of ~1 nm; (ii) J and β values collected from the same SAMs with Ga_2O_3/EGaIn electrodes in the form of tips or microfluidic arrays (i.e., presumably two systems with significantly different amounts and compositions of contaminants) were indistinguishable;[34,87] (iii) J and β values collected from the same SAM with Ga_2O_3/EGaIn tip electrodes in different environments and laboratories (i.e., Harvard University and National University of Singapore) were indistinguishable.[87]

We estimated the influence of organic contamination on the conductivity of the electrode empirically by characterizing junctions of decanethiols formed with Ga_2O_3/EGaIn tips that had been exposed to the ambient atmosphere of our laboratory for different periods of time (1, 5, and 15 min). The plot in Figure 6 compares the $J(V)$ curves from each set (seven replicates; each replicate was a new tip) of these increasingly contaminated $Ag^{TS}-S(CH_2)_9CH_3//Ga_2O_3/EGaIn$ junctions. The 99.9% confidence intervals of all three $J(V)$ curves overlap

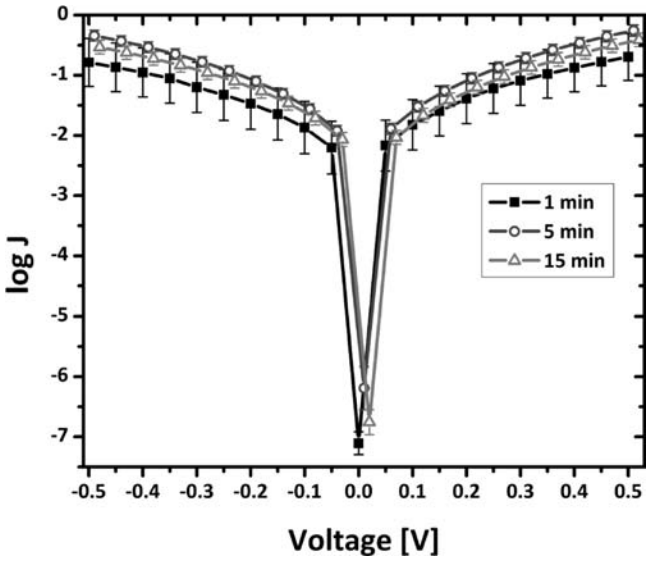

Figure 6. Plot of the $J(V)$ traces obtained from $Ag^{TS}-S(CH_2)_9CH_3//Ga_2O_3/EGaIn$ junctions formed after exposing the $Ga_2O_3/EGaIn$ electrodes to laboratory air for 1 (black filled squares), 5 (dark gray empty circles), and 15 min (gray empty triangles). Error bars correspond to the 99.9% confidence interval for each point. An offset of +0.01 and +0.02 V was applied respectively to the 5 and 15 min data to facilitate comparison of the three traces and their overlapping error bars. The lines are guides to the eye.

across the entire range of voltages. The junctions measured after 1 min of aging were significantly less stable, noisier, and more prone to shorting (yield of 80% after 1 min vs yield of 100% after 5 or 15 min); this instability resulted in a confidence interval that is larger than that of the other two data sets. We interpret the difference in behavior between shorter (1 min) and longer exposures (5 and 15 min) as an effect of the formation of the oxide layer and not as a difference in levels of contamination. A difference in the level of contamination would decrease the mean value of $J(V)$ by increasing the average thickness of the insulating layer, but no significant difference was observed for this last value. *These data suggest that the length of time that the Ga_2O_3/EGaIn electrodes are exposed to ambient conditions does not significantly affect our data within the time frame of our experiments.*

The results in Figure 6 can be explained in at least two ways. (i) The accumulation of organic contaminants is already complete (the rate of adsorption of contaminants decreases strongly over time as the surface energy is gradually reduced by adsorption) after 1 min. This explanation implies that the average rate of adsorption over the first minute of exposure is ~10−70 nm/h, which is 2 orders of magnitude faster than the fastest rate of contamination from laboratory ambient atmosphere that we could find in the literature.[71] (ii) The amount of contamination is negligible during our typical total exposure of an electrode (~5−15 min). This explanation is consistent with published rates of contamination.[88,89] The reason why an incomplete layer of adventitious contaminants would have a negligible effect on the resistance of the junction can be explained by using the electronics analogy defined previously in this discussion. A discontinuous layer of organic contaminants would provide a barrier to charge transport not in the form of a single resistor placed in series with the SAM, but as multiple resistors placed in parallel with the van der Waals interface. The areas with the least resistance will be those where the oxide is in van der Waals contact with the SAM; even if 50% of the surface of the top electrode is covered with adventitious carbon having a resistance much larger than that of the SAM, the measured current density would only decrease by a factor of 2,[12] which is a relatively small uncertainty when compared with the spread in our data.

CONCLUSIONS

The oxide skin formed spontaneously on EGaIn in ambient conditions is apparently passivating, 0.7 nm thick (on average), and mostly composed by Ga_2O_3. Combined data from ARXPS and ToF-SIMS established that the thickness of the oxide on EGaIn after ~1 h of exposure to ambient conditions was, on average, 0.7 nm thick, and composed mostly of Ga_2O_3 (Ga_2O and In_2O_3 exist underneath the Ga_2O_3). This analysis gave no information about the crystallinity of the oxide.

The structure and composition of the $Ag^{TS}-SR//Ga_2O_3$/EGaIn tunneling junctions are conserved, from junction to junction and from tip to tip. To assess the effect of mechanical handling (which is involved in the formation of junctions with Ga_2O_3/EGaIn tips) and of the curvature of the surface, we compared the XPS signals (Ga 3d and In 4d) from an as-fabricated tip (i.e., minimal handling, radius of curvature of ~100 μm) with the same signals originating from drop-shaped samples (i.e., minimal handling, radius of curvature of ~1 cm), and from mechanically deformed tips (i.e., 25 cycles of deformation, radius of curvature of ~100 μm). The ratios of the intensities between the signals originating from the liquid alloy and the oxide were indistinguishable in the three different samples. We inferred that the average thickness of the oxide was comparable among the three samples and, therefore, that mechanical deformations and curvature did not affect the average thickness and composition of the oxide.

The transport of charge through the junction is dominated by the SAM. Previous work on SAM-based tunneling junctions using Ga_2O_3/EGaIn as a top contact yielded consistent values of $J(V)$ for a given alkanethiolate molecule (SC_9-SC_{18}), whenever the number of measurements was statistically significant.[10,34,87] These results suggest that the influence of the Ga_2O_3 skin and of the adventitious adsorbates on the conductivity of the junction is either negligible or similar from junction to junction. The determination of the average thickness of the oxide and adventitious contaminants allowed us to infer the influence of this surface layer on the measurement of current densities from $Ag^{TS}-S-(CH_2)_{n-1}CH_3//Ga_2O_3$/EGaIn tunneling junctions. We compared the resistance of the most conductive junction we measured (10^7 Ω at 0.5 V, for $n = 10$) with the upper bound of the resistance of the surface layer (~1×10^3 Ω) calculated by considering the experimentally determined value of J_0 for $Ag^{TS}-S(CH_2)_{n-1}CH_3//Ga_2O_3$/EGaIn junctions ($10^2$ A/cm^2). Even in this limiting case, the resistance of the junction is larger than that of the surface layer by 4 orders of magnitude; this observation indicates that the surface layer does not affect the measurement of current densities of $Ag^{TS}-S(CH_2)_{n-1}CH_3//Ga_2O_3$/EGaIn junctions. This conclusion is probably not valid for much more conductive SAMs, as has already been suggested in recent reports.[28] The values of resistance and average thickness of the oxide reported here will be useful in evaluating the impact of the surface layer on the measurement of current densities from highly "conductive" SAMs.

Exposure of the electrode to adventitious contaminants found in laboratory atmosphere does not significantly change the conductivity of the junction over the time required to measure tunneling currents through SAMs. Adventitious contaminants also adsorb on the tip, as suggested by the amount of carbon detected by XPS on Ga_2O_3/EGaIn electrodes. We measured the conductivity of $Ag^{TS}-S(CH_2)_9CH_3//Ga_2O_3$/EGaIn junctions formed after exposing the Ga_2O_3/EGaIn electrodes to laboratory atmosphere for 1, 5, and 15 min. These times are representative of the typical exposure a tip undergoes in a typical junction experiment. The $J(V)$ values for all three conditions were within the 99.9% confidence interval of each other. We infer that, at such levels of exposure, either the amount of adventitious contamination on the surface is negligible or it is constant.

The Ga_2O_3/EGaIn interface is rough at the micrometer scale. Simultaneous ToF-SIMS mapping and Ar ion sputtering of the surface of a frozen Ga_2O_3/EGaIn drop yielded tomographic maps of the lateral distribution of oxide as function of depth. Our results show that, while most of the oxide is ~0.7 nm in thickness, the Ga_2O_3/EGaIn interface exhibits a micrometer-scale roughness, characterized by thread-like strands of oxide, ~4 μm wide and several micrometers thick. It appears, however, that this roughness——and the effective contact area of the junction——is constant from junction to junction, since the values of $J(V)$ are reproducible.

In^{3+} segregates at the interface between the bulk liquid alloy and the rigid oxide. High-resolution ARXPS analysis of drop samples identified the In^{3+} species as being segregated between the oxide and the liquid metal alloy. This finding is consistent with the lower surface tension of In compared with Ga, and with previous results by our group[53] and others.[66,90]

■ ASSOCIATED CONTENT

Supporting Information

Detailed methods and supplementary definitions and discussion. This material is available free of charge via the Internet at http://pubs.acs.org.

■ AUTHOR INFORMATION

Corresponding Author

*E-mail: gwhitesides@gmwgroup.harvard.edu (G.M.W.); rns.sodhi@utoronto.ca (R.N.S.S.); peter.brodersen@utoronto.ca (P.B.).

Notes

The authors declare no competing financial interest.

■ ACKNOWLEDGMENTS

The initial stages of this work (2008–2010) were supported by NSF Award No. CHE-0518055. After 2010, the remainder of the work (~60%) was supported by a subcontract from a DoE award to Northwestern University (DE-SC0000989). L.C. thanks NSERC for a postdoctoral fellowship. M.M.T. was supported by a Mary Fieser postdoctoral fellowship and a postdoctoral fellowship from the Nanoscience and Engineering Center at Harvard University. Surface Interface Ontario gratefully acknowledges the support of both the Canadian Foundation for Innovation and the Ontario Research Fund.

■ REFERENCES

(1) Chiechi, R. C.; Weiss, E. A.; Dickey, M. D.; Whitesides, G. M. *Angew. Chem., Int. Ed. Engl.* **2008**, *47*, 142–144.
(2) Akkerman, H. B.; Blom, P. W. M.; de Leeuw, D. M.; de Boer, B. *Nature* **2006**, *441*, 69–72.
(3) Akkerman, H. B.; Kronemeijer, A. J.; van Hal, P. A.; de Leeuw, D. M.; Blom, P. W. M.; de Boer, B. *Small* **2008**, *4*, 100–104.
(4) Beebe, J. M.; Engelkes, V. B.; Miller, L. L.; Frisbie, C. D. *J. Am. Chem. Soc.* **2002**, *124*, 11268–11269.
(5) Chu, C. W.; Na, J. S.; Parsons, G. N. *J. Am. Chem. Soc.* **2007**, *129*, 2287–2296.
(6) Engelkes, V. B.; Beebe, J. M.; Frisbie, C. D. *J. Am. Chem. Soc.* **2004**, *126*, 14287–14296.
(7) Haick, H.; Cahen, D. *Acc. Chem. Res.* **2008**, *41*, 359–366.
(8) Holmlin, R. E.; Haag, R.; Chabinyc, M. L.; Ismagilov, R. F.; Cohen, A. E.; Terfort, A.; Rampi, M. A.; Whitesides, G. M. *J. Am. Chem. Soc.* **2001**, *123*, 5075–5085.
(9) Love, J. C.; Estroff, L. A.; Kriebel, J. K.; Nuzzo, R. G.; Whitesides, G. M. *Chem. Rev.* **2005**, *105*, 1103–1169.
(10) Thuo, M. M.; Reus, W. F.; Nijhuis, C. A.; Barber, J. R.; Kim, C.; Schulz, M. D.; Whitesides, G. M. *J. Am. Chem. Soc.* **2011**, *133*, 2962–2975.
(11) Ulman, A. *Chem. Rev.* **1996**, *96*, 1533–1554.
(12) Weiss, E. A.; Chiechi, R. C.; Kaufman, G. K.; Kriebel, J. K.; Li, Z. F.; Duati, M.; Rampi, M. A.; Whitesides, G. M. *J. Am. Chem. Soc.* **2007**, *129*, 4336–4349.
(13) Nijhuis, C. A.; Reus, W. F.; Whitesides, G. M. *J. Am. Chem. Soc.* **2009**, *131*, 17814–17827.
(14) Stein, N.; Korobko, R.; Yaffe, O.; Lavan, R. H.; Shpaisman, H.; Tirosh, E.; Vilan, A.; Cahen, D. *J. Phys. Chem. C* **2010**, *114*, 12769–12776.
(15) Akkerman, H. B.; de Boer, B. *J. Phys.: Condens. Matter* **2008**, *20*, No. 013001.
(16) Akkerman, H. B.; Kronemeijer, A. J.; Harkema, J.; van Hal, P. A.; Smits, E. C. P.; de Leeuw, D. M.; Blom, P. W. M. *Org. Electron.* **2010**, *11*, 146–149.
(17) Akkerman, H. B.; Naber, R. C. G.; Jongbloed, B.; van Hal, P. A.; Blom, P. W. M.; de Leeuw, D. M.; de Boer, B. *Proc. Natl. Acad. Sci. U.S.A.* **2007**, *104*, 11161–11166.
(18) Engelkes, V. B.; Beebe, J. M.; Frisbie, C. D. *J. Phys. Chem. B* **2005**, *109*, 16801–16810.
(19) Bonifas, A. P.; McCreery, R. L. *Nat. Nanotechnol.* **2010**, *5*, 612–617.
(20) Holmlin, R. E.; Ismagilov, R. F.; Haag, R.; Mujica, V.; Ratner, M. A.; Rampi, M. A.; Whitesides, G. M. *Angew. Chem., Int. Ed. Engl.* **2001**, *40*, 2316.
(21) Rampi, M. A.; Whitesides, G. M. *Chem. Phys.* **2002**, *281*, 373–391.
(22) Simeone, F. C.; Rampi, M. A. *Chimia* **2010**, *64*, 362–369.
(23) Slowinski, K.; Chamberlain, R. V.; Miller, C. J.; Majda, M. *J. Am. Chem. Soc.* **1997**, *119*, 11910–11919.
(24) Slowinski, K.; Fong, H. K. Y.; Majda, M. *J. Am. Chem. Soc.* **1999**, *121*, 7257–7261.
(25) Slowinski, K.; Majda, M. *J. Electroanal. Chem.* **2000**, *491*, 139–147.
(26) York, R. L.; Nguyen, P. T.; Slowinski, K. *J. Am. Chem. Soc.* **2003**, *125*, 5948–5953.
(27) York, R. L.; Slowinski, K. *J. Electroanal. Chem.* **2003**, *550*, 327–336.
(28) Fracasso, D.; Valkenier, H.; Hummelen, J. C.; Solomon, G. C.; Chiechi, R. C. *J. Am. Chem. Soc.* **2011**, *133*, 9556–9563.
(29) Paul, A.; Watson, R. M.; Wierzbinski, E.; Davis, K. L.; Sha, A.; Achim, C.; Waldeck, D. H. *J. Phys. Chem. B* **2010**, *114*, 14140–14148.
(30) Khoshtariya, D. E.; Dolidze, T. D.; Shushanyan, M.; Davis, K. L.; Waldeck, D. H.; van Eldik, R. *Proc. Natl. Acad. Sci. U.S.A.* **2010**, *107*, 2757–2762.
(31) Davis, K. L.; Drews, B. J.; Yue, H.; Waldeck, D. H.; Knorr, K.; Clark, R. A. *J. Phys. Chem. C* **2008**, *112*, 6571–6576.

(32) Yue, H. J.; Waldeck, D. H.; Schrock, K.; Kirby, D.; Knorr, K.; Switzer, S.; Rosmus, J.; Clark, R. A. *J. Phys. Chem. C* **2008**, *112*, 2514−2521.
(33) French, S. J.; Saunders, D. J.; Ingle, G. W. *J. Phys. Chem.* **1938**, *42*, 265−274.
(34) Nijhuis, C. A.; Reus, W. F.; Barber, J. R.; Dickey, M. D.; Whitesides, G. M. *Nano Lett.* **2010**, *10*, 3611−3619.
(35) Nijhuis, C. A.; Reus, W. F.; Whitesides, G. M. *J. Am. Chem. Soc.* **2010**, *132*, 18386−18401.
(36) Reed, M. A.; Zhou, C.; Muller, C. J.; Burgin, T. P.; Tour, J. M. *Science* **1997**, *278*, 252−254.
(37) Chen, F.; Hihath, J.; Huang, Z. F.; Li, X. L.; Tao, N. J. *Annu. Rev. Phys. Chem.* **2007**, *58*, 535−564.
(38) Haag, R.; Rampi, M. A.; Holmlin, R. E.; Whitesides, G. M. *J. Am. Chem. Soc.* **1999**, *121*, 7895−7906.
(39) Mishchenko, A.; Vonlanthen, D.; Meded, V.; Burkle, M.; Li, C.; Pobelov, I. V.; Bagrets, A.; Viljas, J. K.; Pauly, F.; Evers, F. *Nano Lett.* **2010**, *10*, 156−163.
(40) Xu, B. Q.; Tao, N. J. J. *Science* **2003**, *301*, 1221−1223.
(41) Venkatramani, R.; Davis, K. L.; Wierzbinski, E.; Bezer, S.; Balaeff, A.; Keinan, S.; Paul, A.; Kocsis, L.; Beratan, D. N.; Achim, C. *J. Am. Chem. Soc.* **2011**, *133*, 62−72.
(42) Wold, D. J.; Frisbie, C. D. *J. Am. Chem. Soc.* **2001**, *123*, 5549−5556.
(43) Mahmoud, A. M.; Bergren, A. J.; Pekas, N.; McCreery, R. L. *Adv. Funct. Mater.* **2011**, *21*, 2273−2281.
(44) McCreery, R. L.; Wu, J.; Kalakodimi, R. P. *Phys. Chem. Chem. Phys.* **2006**, *8*, 2572−2590.
(45) Bergren, A. J.; Harris, K. D.; Deng, F. J.; McCreery, R. L. *J. Phys.: Condens. Matter* **2008**, *20*, No. 374117.
(46) Yan, H. J.; McCreery, R. L. *ACS Appl. Mater. Interfaces* **2009**, *1*, 443−451.
(47) Chen, J.; Reed, M. A.; Rawlett, A. M.; Tour, J. M. *Science* **1999**, *286*, 1550−1552.
(48) Kim, T. W.; Wang, G.; Lee, H.; Lee, T. *Nanotechnology* **2007**, *18*, No. 315204.
(49) Venkataraman, L.; Klare, J. E.; Nuckolls, C.; Hybertsen, M. S.; Steigerwald, M. L. *Nature* **2006**, *442*, 904−907.
(50) Stewart, D. R.; Ohlberg, D. A. A.; Beck, P. A.; Chen, Y.; Williams, R. S.; Jeppesen, J. O.; Nielsen, K. A.; Stoddart, J. F. *Nano Lett.* **2004**, *4*, 133−136.
(51) Valkenier, H.; Huisman, E. H.; van Hal, P. A.; de Leeuw, D. M.; Chiechi, R. C.; Hummelen, J. C. *J. Am. Chem. Soc.* **2011**, *133*, 4930−4939.
(52) Fatemi, V.; Kamenetska, M.; Neaton, J. B.; Venkataraman, L. *Nano Lett.* **2011**, *11*, 1988−1992.
(53) Dickey, M. D.; Chiechi, R. C.; Larsen, R. J.; Weiss, E. A.; Weitz, D. A.; Whitesides, G. M. *Adv. Funct. Mater.* **2008**, *18*, 1097−1104.
(54) Larsen, R. J.; Dickey, M. D.; Whitesides, G. M.; Weitz, D. A. *J. Rheol.* **2009**, *53*, 1305−1326.
(55) Sek, S.; Bilewicz, R.; Slowinski, K. *Chem. Commun.* **2004**, 404−405.
(56) Chen, F.; Li, X.; Hihath, J.; Huang, Z. F.; Tao, N. J. *J. Am. Chem. Soc.* **2006**, *128*, 15874−15881.
(57) Haiss, W.; Nichols, R. J.; van Zalinge, H.; Higgins, S. J.; Bethell, D.; Schiffrin, D. J. *Phys. Chem. Chem. Phys.* **2004**, *6*, 4330−4337.
(58) Suzuki, M.; Fujii, S.; Fujihira, M. *Jpn. J. Appl. Phys., Part 1* **2006**, *45*, 2041−2044.
(59) Cui, X. D.; Primak, A.; Zarate, X.; Tomfohr, J.; Sankey, O. F.; Moore, A. L.; Moore, T. A.; Gust, D.; Nagahara, L. A.; Lindsay, S. M. *J. Phys. Chem. B* **2002**, *106*, 8609−8614.
(60) Morita, T.; Lindsay, S. *J. Am. Chem. Soc.* **2007**, *129*, 7262.
(61) Reus, W. F.; Nijhuis, C. A.; Barber, J. R.; Thuo, M. M.; Tricard, S.; Kim, C.; Whitesides, G. M. *J. Phys. Chem. C* **2012**, *116*, 6714−6733.
(62) Liao, J.; Bernard, L.; Langer, M.; Schonenberger, C.; Calame, M. *Adv. Mater.* **2006**, *18*, 2444.
(63) Regan, M. J.; Tostmann, H.; Pershan, P. S.; Magnussen, O. M.; DiMasi, E.; Ocko, B. M.; Deutsch, M. *Phys. Rev. B* **1997**, *55*, 10786−10790.
(64) Tostmann, H.; DiMasi, E.; Pershan, P. S.; Ocko, B. M.; Shpyrko, O. G.; Deutsch, M. *Phys. Rev. B* **1999**, *59*, 783−791.
(65) Scharmann, F.; Cherkashinin, G.; Breternitz, V.; Knedlik, C.; Hartung, G.; Weber, T.; Schaefer, J. A. *Surf. Interface Anal.* **2004**, *36*, 981−985.
(66) Dumke, M. F.; Tombrello, T. A.; Weller, R. A.; Housley, R. M.; Cirlin, E. H. *Surf. Sci.* **1983**, *124*, 407−422.
(67) For unreacted liquid metal alloys, the Gibbs adsorption rule predicts that the component with the lowest surface tension (0.881−1.100 $J{\cdot}m^{-2}$ for Ga, 0.675−0.700 $J{\cdot}m^{-2}$ for In[91,92]) will segregate to the surface.[90] For example, a single monolayer of almost pure indium (94 atom %) is found on the surface of EGaIn.[66,90] Similar segregation is also observed in Ga−Bi and other alloys.[90]
(68) Lorenz, M. R.; Woods, J. F.; Gambino, R. J. *J. Phys. Chem. Solids* **1967**, *28*, 403.
(69) Passlack, M.; Schubert, E. F.; Hobson, W. S.; Hong, M.; Moriya, N.; Chu, S. N. G.; Konstadinidis, K.; Mannaerts, J. P.; Schnoes, M. L.; Zydzik, G. J. *J. Appl. Phys.* **1995**, *77*, 686−693.
(70) Paterson, G. W.; Wilson, J. A.; Moran, D.; Hill, R.; Long, A. R.; Thayne, I.; Passlack, M.; Droopad, R. *Mater. Sci. Eng., B* **2006**, *135*, 277−281.
(71) Strein, E.; Allred, D. *Thin Solid Films* **2008**, *517*, 1011−1015.
(72) Strein, E. Studying and Eliminating Adventitious Carbon Contamination on Silicon Wafers. B.Sc., Brigham Young University, Provo, UT, 2008.
(73) Wagner, C. D.; Naumkin, A. V.; Kraut-Vass, A.; Allison, J. W.; Powell, C. J.; Rumble, J. R. J. NIST X-ray Photoelectron Spectroscopy Database, 3.5th ed.; 2007.
(74) In the case of ARXPS, the signal from the tips did not show any meaningful dependence on the angle of collection, most likely due to the difficulty of gathering angle-dependent information with a spot size (100 μm) which was comparable to the radius of curvature (100 μm) of the surface. In the case of ToF-SIMS, it was not possible to collect reliable profile information from such a small area with such high curvature.
(75) Beard, B. C.; Brizzolara, R. A. *J. Vac. Sci. Technol., A* **1996**, *14*, 89−94.
(76) Brizzolara, R. A.; Beard, B. C. *Surf. Interface Anal.* **1999**, *27*, 716−727.
(77) Saheli, G.; Conti, G.; Uritsky, Y.; Foad, M. A.; Brundle, C. R.; Mack, P.; Kouzminov, D.; Werner, M.; van den Berg, J. A. *J. Vac. Sci. Technol., B* **2008**, *26*, 298−304.
(78) Jedral, L.; Ruda, H. E.; Sodhi, R.; Ma, H.; Mannik, L. *Can. J. Phys.* **1992**, *70*, 1050−1056.
(79) We interpreted this observation as caused by a difference in the thermal expansion coefficients of the oxide and the metal (metal > oxide), which caused the metal to shrink more rapidly than the oxide upon cooling.
(80) Barr, T. L.; Seal, S. *J. Vac. Sci. Technol., A* **1995**, *13*, 1239−1246.
(81) Piao, H.; McIntyre, N. S. *Surf. Interface Anal.* **2002**, *33*, 591−594.
(82) Simmons, J. G. *J. Appl. Phys.* **1963**, *34*, 1793.
(83) The voltage is present in the full form of the Simmons equation. This "reduced" form is a rather crude approximation used to fit data from SAM-based tunneling barriers.
(84) Akkerman, H. B. Large-Area Molecular Junctions. Ph.D. Dissertation, University of Groningen, Groningen, Netherlands, 2008; Chapter 7.
(85) Wang, G.; Kim, Y.; Na, S.-I.; Kahng, Y. H.; Ku, J.; Park, S.; Jang, Y. H.; Kim, D.-Y.; Lee, T. *J. Phys. Chem. C* **2011**, *115*, 17979−17985.
(86) Haran, A.; Waldeck, D. H.; Naaman, R.; Moons, E.; Cahen, D. *Science* **1994**, *263*, 948−950.
(87) Nijhuis, C. A.; Reus, W. F.; Barber, J. R.; Whitesides, G. M. *J. Phys. Chem. C*, in press; DOI: 10.1021/jp303072a.
(88) Veillerot, M.; Danel, A.; Cetre, S.; Tardif, F. *Mater. Sci. Eng., B* **2003**, *102*, 385−389.
(89) Seah, M. P.; Spencer, S. J. *J. Vac. Sci. Technol., A* **2003**, *21*, 345−352.

(90) Tostmann, H.; DiMasi, E.; Ocko, B. M.; Deutsch, M.; Pershan, P. S. *J. Non-Cryst. Solids* **1999**, *250*, 182−190.
(91) Tyson, W. R.; Miller, W. A. *Surf. Sci.* **1977**, *62*, 267−276.
(92) de Boer, F. R.; Boom, R.; Mattens, W. C. M.; Miedema, A. R.; Niessen, A. K. *Cohesion in Metals*; North-Holland: Amsterdam, 1988.